On the Need for Bump Event Correction in Vibration Test Profiles Representing Road Excitations in Automobiles *

A. Steinwolf, J.A. Giacomin, and W.J. Staszewski
Department of Mechanical Engineering, University of Sheffield, United Kingdom

Abstract: This paper presents an approach to the synthesis of compressed vibration test profiles representing much longer time histories obtained in road testing of ground vehicles. Vibration test profiles are defined as those related directly to operational testing on specific road surfaces and which summarise the input to the vehicle in the given conditions. The method extends classical Fourier transform technique by means of bump event correction in the background Fourier signal where the bump event term implies a high-amplitude transient event of the shock type. The orthogonal wavelet decomposition was used as a specific filtering tool facilitating bump event identification. Examples of seat guide vertical acceleration have been considered. Calculated probability density functions suggest the ability of the bump correction method to improve the statistical accuracy of the final vibration test profile with respect to the original road data. Test profiles obtained by means of Fourier transform synthesis with subsequent reinsertion of bump events from separated frequency bands were more accurate than those obtained by Fourier synthesis alone. Further developments led to advanced bump reinsertion with synchronisation of events occurring in different frequency bands at the same moment of time. Test profiles generated in this way have provided better accuracy compared to the non-synchronised algorithm.

Keywords: vibration test profile, vehicle, in-house testing, wavelet analysis, bump events, shocks, probability density function tails.

---

* Accepted for publication in the Journal of Automobile Engineering,
Proceedings of the Institution of Mechanical Engineers, Part D

NOTATION:

a	dilation (scale parameter)
a_i	(i = 1, 2, …) wavelet coefficient amplitude
a_o	dilation step
b	translation (time parameter)
b_o	translation step
c_k	coefficients of the non-recursive part of the IIR digital filter
d_k	coefficients of the recursive part of the IIR digital filter
f	frequency
i	$\sqrt{-1}$
j, k, m, m^1, n, n^1	integer numbers
L	number of time points in road data time history
t	time
Δt	time step when converting signals to digital form
$W\psi$	wavelet transform
$X(f)$	frequency domain signal
$x(t)$	time domain signal
$y(t)$	output signal from the IIR digital filter
y_j	discrete time point of the output signal
$z(t)$	input signal to the IIR digital filter
z_j	discrete time point of the input signal
σ	r.m.s value of time domain signal
ψ	wavelet function
$\psi_{a,b}$	dilated and translated wavelet function
*	complex conjugate

1. INTRODUCTION

Vibration test signals are important tools for both automotive durability and automotive comfort development programs. Such activities make extensive use of road measurements, numerical simulations, and laboratory testing. Both numerical simulation and experimental testing require reference input excitation signals which represent real operating conditions and which contain the features necessary to evidence any problematic behaviour of the system under consideration.

Since several operating conditions are typically of interest, and since the complexity and cost of the laboratory tests can be great, restrictions are usually placed on the allowable time duration of the vibration test signals used. A particular scenario is the comfort testing of vehicle components involving human subjects. Vibration test simulators are often used to test subjective reaction to the vibration of seats, steering, or other vehicle components. Human short term memory can typically hold ambient stimuli for durations of not more than 10-20 seconds [**1**]. Therefore, a direct time waveform reproduction of road recordings is not appropriate and shorter test profiles are required which should be representative of the principal vibrational features encountered by the vehicle in much longer road measurements.

To properly describe vibration data acquired during vehicle operation, a random process model is necessary in most cases. A traditional approach to the numerical or experimental simulation of random data of variable length is to implement the power spectral density (PSD), which is supposed to completely represent the vibration process under consideration. The advantages of the PSD presentation are convincing because one has an immediate view of frequency decomposition of the vibration.

Test methodologies based on PSD analysis rely on the fact that a time history for shaker testing or Monte Carlo numerical simulation can be reconstructed from the prescribed PSD by the inverse Fourier transform. This is the basic procedure [**2,3,4**] used in random controllers for shakers and similar test benches. The procedure permits the reproduction of any stationary random excitation matching precisely the PSD of road data prescribed. The phase shifts between harmonics of the Fourier series are chosen in a random manner as stochastic variables uniformly distributed in the $[0,2\pi]$ interval. This makes the obtained signal random and provides an opportunity of generating any number of different time history samples of arbitrary length with the same PSD.

Theory of random processes states that the time histories of the same random process are always different (not repeatable) for each new sample. The process itself is not identified by means of the time history but by means of specific characteristics like probability density functions, moments, auto- and cross-correlation functions and, of course, the PSD. That is why, if the PSD is matched, the synthetic signal obtained can be considered equivalent to the road excitation, even though the initial road data record will never be repeated. This is commonly used as a justification of the inverse PSD approach. The authors support this point of view only in the case if the vibration under consideration is completely described by the PSD. This is not always the case and, in response to this fact, some modifications of the inverse Fourier transform shaker simulation method have been suggested [**5,6,7,8**].

The applicability of the PSD-based approach should always be checked in each particular case because exceptions to the PSD rule might be quite impressive and surprisingly more frequent than one would expect. The top plot in Fig. 1,a is a time history of vertical acceleration measured at the rear mounting bolt of the driver seat in a Renault automobile on a country road test track (concrete with very damaged surface). This vibration record consisted of several repetitive runs on the same track. The measurements were transferred to digital form with a sampling rate of 409.6 Hz and a PSD characteristic was computed.

The obtained PSD function (shown by solid curve in Fig. 2*) was taken as a source material for time history simulation by the inverse Fourier procedure. The resulting time history is presented in Fig. 1,b and its PSD is shown by the dotted curve in Fig. 2. While the power spectral densities of the road data and the synthetic signal (solid and dotted curves in Fig. 2) are so close that are not distinguishable for most of frequencies, the time histories presented in Fig. 1 show how erroneous is the PSD simulation of these road data. Due to the essential differences in signal peak amplitudes (as much as 50% for positive peaks), the impact of these two excitations on the structural fatigue of automobile components and on human comfort in the car would be expected to be quite different.

The presence of numerous bump events (high-amplitude transient events of the shock type) is common in time histories of ground vehicle vibration. The effect had been noticed first for heavy wheeled and tracked vehicles [**9,10**] on rough roads and then for automobiles [**5,11**] as well. When a car or truck is moving over a considerable separate irregularity of the road, a high peak, well above the average level, occurs in the vibration record. A pothole is an extreme situation of this kind, however even those roads which are smooth at first glance normally have rougher points that produce bump impacts. When this happens the time history of excitation acting on the passengers and the vehicle structure includes occasional high spikes of random intensity. That is what is visible in Fig. 1,a with the road data and is absent in Fig. 1,b with the synthetic signal. The latter is, therefore, a reproduction of road frequency content in terms of PSD (see Fig. 2) but not a simulation of the road data as a real excitation.

It should be pointed out that in many cases the situation with bump event presence in road data might not be as clear as in Fig. 1. It is typical that a PSD of operational vibration of the type shown in Fig. 2 consists of a series of resonances due to the vibrational behaviour of different subsystems of the vehicle. The first resonance with its slopes stretched in the region from 0 to 5 Hz is common in any road data and relates to the rigid body motion of the car chassis on the main suspensions. The second broader resonance (covering frequencies from 5 to 13 Hz) can be associated with the behaviour of suspension units separately or with the rigid body motion of the engine/gearbox. The third resonance distributed between 13 and 22 Hz may reflect the low-frequency flexible body modes of the chassis. Finally, the fourth broadest region (including frequencies from 22 to 60 Hz) is probably defined by higher-frequency modes of the chassis and by tire resonances.

Each of the above (or similar in other vehicles) frequency bands may generate its own bump events which are different in number and sharpness. However, these events related to the behaviour of one subsystem may be mixed with, and even fully covered by, a vibration signal component from another frequency band. Thus smaller bump events which are specific and essential for behaviour of a certain subsystem can be missed, if analysing and simulating the measured vibration as a whole. Since any bump inputs to the vehicle can potentially be important, the main objectives of the research described in this paper were to

- preserve bump events inherent to each of the vehicle subsystem frequency bands contributing to the entire road vibration
- properly reflect every type of bump event when generating shaker test profiles (also called “vibration missions” in [**11,12**]).

This was achieved by implementation of the wavelet analysis tool that is explained in the next section.

---

* *The first peak of the PSD curve at 1.6 Hz appeared to be so much higher than others that it was impossible to present all peaks on the same plot. Thus, in Fig. 2 the vertical axis scale is chosen in such a way that the vertex of the first peak in the PSD is clipped for the sake of making other peaks visible. The whole view of the first peak is presented below in Fig. 6,h.*

2. WAVELET ANALYSIS

The wavelet transform is a linear transformation that decomposes a given function into a superposition of elementary functions. Wavelets represent a natural extension of the classic Fourier analysis. The classical Fourier transform defined as

$$X(f) = \int_{-\infty}^{+\infty} x(t) e^{-i2\pi f t} dt \tag{1}$$

decomposes a signal into linear combination of an infinite sum of elementary sine and cosine functions (Fig. 3,a). This transformation leads from the time domain, where the vibration signal is originally defined, to a new spectral representation in the frequency domain. Fourier analysis is used in many engineering applications from modelling to prediction. However, it is not well suited to nonstationary data. Many attempts have been made to overtake this drawback. The analysis in both time and frequency domains using the so-called windowed Fourier transform is the first important development. In contrast to the Fourier transform, the windowed Fourier transform decomposes a signal partially using finite sine and cosine waves. These finite elementary functions represent the window function. The size of this window is fixed, however, the number of oscillations of sine and cosine waves within the window varies (Fig. 3,b).

Wavelets represent a natural extension of this approach. Similarly to the Fourier transform, the basic elementary functions used in wavelet analysis oscillate and thus resemble waves. Also, following the windowed Fourier transform, these waves decay to zero. However, in contrast to the windowed Fourier transform the number of oscillations for each decaying wave is constant (Fig. 3,c). The continuous wavelet transform can be defined as

$$W\psi(a,b) = \frac{1}{\sqrt{a}} \int_{-\infty}^{+\infty} x(t) \psi^* \left(\frac{t-b}{a} \right) dt \tag{2}$$

where b is a translation indicating the locality, a is a dilation or scale parameter, $\psi(t)$ is an analysing or elementary wavelet and $\psi^*(.)$ is the complex conjugate of $\psi(.)$. Each value of the wavelet transform $W\psi(a, b)$ in Equation (2) is normalised by the factor $1/\sqrt{a}$. This normalisation ensures the integral energy given by each wavelet $\psi_{a,b}(t)$ is independent of the dilation a. Mathematically wavelet analysis is a linear transformation which uses wavelets for decomposition of a function. By compression and stretching of wavelets which are scaling operations one adapts them to the analysed function. Compressed wavelets (small window) can see better short-lived high frequency components and stretched wavelets (large window) can analyse better long-lived low frequency parts of the signal.

In the continuous wavelet transform a one-dimensional signal is transformed into a two-dimensional continuous time-scale (time-frequency) grid. Clearly, this imposes redundancy in the analysis and the question is whether it is possible to limit the transform to a subset of wavelet coefficients on this grid and still recover the original signal. The discretisation of the time b and scale a in Equation (2) leads to the discrete wavelet transform. A natural way of discretising the continuous time-scale wavelet grid (a,b) is to set,

$$a = a_0^m, \qquad b = n\ a_0^n b_0 \tag{3}$$

where m, n are integers and $b_0 \neq 0$ is the translation step. This implies that the continuous wavelets $\psi_{a,b}(t)$ in Equation (2) become discrete wavelets given by,

$$\psi_{m,n}(t) = a_0^{-m/2}\psi\left(a_0^{-m}t - nb_0\right) \tag{4}$$

It follows that the discrete wavelet transform can now be defined as,

$$W\psi(m,n) = \int_{-\infty}^{+\infty} x(t)\psi_{m,n}^{*}(t)dt \tag{5}$$

The higher the subsampling on this grid, the smaller the redundancy of the wavelet transform. When the wavelets $\psi_{m,n}(t)$ form a set of orthonormal functions, there is no redundancy in the analysis and the discrete wavelet transform given by Equation (5) becomes the orthogonal wavelet transform. Here the orthonormality means that the inner product $\left\langle \psi_{m,n,}\psi_{m^1,n^1} \right\rangle$ satisfies,

$$\left\langle \psi_{m,n,}\psi_{m^1,n^1} \right\rangle = \begin{cases} 1 \;\; for \quad m = m^1 \quad and \quad n = n^1 \\ 0 \;\; otherwise \end{cases} \tag{6}$$

and the wavelets are normalised.

Any arbitrary signal $x(t)$ can be then represented as a weighted sum of orthogonal wavelets,

$$x(t) = \sum_m \sum_n W_\psi(m,n)\psi_{m,n}(t) \tag{7}$$

A number of different bases have been proposed to construct orthogonal wavelets. The simpliest basis can be given by the well known Haar function . Much more effective analysis and synthesis can be obtained with the wavelets of Daubechies [**13**], used in this paper.

The orthogonal wavelet transform gives the span of the analysed data in a form of the so-called wavelet levels, at different resolutions according to wavelet scales. In order to explain wavelet levels it is convenient to limit the analysis of any arbitrary function $x(t)$ to the interval $0 \leq t < 1$ and introduce the circular wavelet transform. This can be done similarly to the discrete Fourier transform [**14**], where $x(t)$, $0 \leq t < 1$, is regarded as one period of the signal so that $x(t)$ can be repeated in the adjacent unit intervals. In the same way wavelets can be wrapped around the analysed interval. Also, it can be shown that the sum of all contributions in Equation (7) for $m \leq -1$ is constant [**14**]. Under all these assumptions, the wavelet decomposition of $x(t)$ in the analysed interval $0 \leq t < 1$ takes the form of a matrix series [**14**],

$$x(t) = a_0\phi(t) + a_1\psi(t) + \begin{vmatrix} a_2 & a_3 \end{vmatrix} \begin{vmatrix} \psi(2t) \\ \psi(2t-1) \end{vmatrix} +$$

$$+ \begin{vmatrix} a_4 & a_5 & a_6 & a_7 \end{vmatrix} \begin{vmatrix} \psi(4t) \\ \psi(4t-1) \\ \psi(4t-2) \\ \psi(4t-3) \end{vmatrix} + \ldots + a_{2^m+n}\,\psi\left(2^m t - n\right) + \ldots \tag{8}$$

where the coefficients $a_0\, a_1, a_2, a_3, \ldots$ give the amplitude of all contributing wavelets. This clearly shows that the analysed signal $x(t)$ can be represented as a sum of so called wavelet levels given by,

$$x_m(t) = \begin{cases} a_0\ \phi(t) & \text{for} \quad m = -1 \\ \sum_n \ a_{2^m+n}\ \psi\left(2^m t - n\right) & \text{for} \quad m = 0,\ 1,\ 2,\ 3,\ \ldots \end{cases} \tag{9}$$

All levels are in fact reconstructed time-domain signals from the wavelet decomposition. Each $x_m(t)$ level displays a different frequency band and gives a contribution to the whole signal energy. Since the scale (frequency) partitioning leads to a partitioning in the time domain that is finer in the higher frequency bands, lower levels correspond to low frequencies whereas higher levels exhibit high frequencies of the signal.

The sum of all levels recreates the original signal, i.e.

$$x(t) = \sum_m \ x_m(t) \tag{10}$$

Although the wavelet levels are in the time domain, this orthogonal decomposition allows one not only for time domain localisation of different events in the signal but also for frequency decomposition of different signal components. The wavelet analysis has found several applications to automobile vibration experimental data, e.g. Ref. [**11,15,16**].

3. IMPLEMENTATION OF ORTHOGONAL WAVELETS FOR PRESERVING BUMP EVENTS WHEN SEPARATING VIBRATION COMPONENTS

Along with vibration data compression and denoising [**17,18**], the orthogonal wavelet transform is suitable for selection of different signal components. The choice of specific wavelet coefficients corresponding to one or several adjacent wavelet levels, while all other coefficients are set to zero, can remove lower and higher frequency components and leave only that particular frequency band which is of interest. In what follows, the filtering based on wavelets is discussed and a comparison between the classical filtering procedure and wavelet-based procedure is presented.

As discussed in the Introduction, the behaviour of each of the vehicle subsystems contributing to the road vibration has its own frequency range and, therefore, can be distinguished by analyzing the power spectral density. However, it is not so easy to actually separate one particular subsystem behaviour and to obtain an individual time history. Separation is often performed by means of digital filters [**19**], particularly in the Infinite Impulse Response (IIR) form given by

$$y_j = c_0 z_j + \sum_{k=1}^{n} \left(c_k z_{j-k} + d_k y_{j-k} \right) \tag{11}$$

According to the above equation each time point in the filtered output $y_j = y(j\Delta t)$ is computed not only via the corresponding input value z_j, but several preceding points of the input z_{j-k} and output y_{j-k} are also involved. Employing Equation (11) for the next time history point y_{j+1}, one can see that, if a bump peak occurred at the time moment $j\Delta t$, then the difference between output peak value y_j and the next point y_{j+1} (i.e. sharpness of the peak)

$$y_j - y_{j+1} = c_0 (z_j - z_{j+1}) + \sum_{k=1}^{n} \left\{ c_k (z_{j-k} - z_{j-k+1}) + d_k (y_{j-k} - y_{j-k+1}) \right\} \tag{12}$$

depends not only on this difference for input $(z_j - z_{j+1})$ at the same moment of time but on other time history points z_{j-k} $k = \overline{1,n}$ as well. This is a source of additional error in peak reproduction and might make bump events in the filtered signal component different from those in the road data when this component is mixed with other ones.

The thin curve in Fig. 4 presents a short and magnified section of the road data described in Fig. 1,a. For these data, four frequency bands chosen from the PSD of Fig. 2 (and related to behaviour of different subsystems of a vehicle) have been separated and, for each of them, two competing time histories were obtained by means of two numerical procedures: orthogonal wavelet decomposition (Daubechies 12-th order wavelets) and a 50-th order band-pass digital filter corresponding to a Butterworth analog filter.

Results for the highest frequency band (from 22 to 60 Hz) are presented in Figs. 5,a by the thin curve for wavelet decomposition and the thick curve for Butterworth digital filtering. Differences between the curves are evident and it is clear that the bump behaviour has been affected by the band-pass filter. This error of smoothing time history peaks is present to a greater or lesser extent when extracting other frequency bands as seen in Figs. 5,b,c,d. In this example the time histories obtained by wavelet decomposition always had sharper peaks than those obtained by Butterworth filtering*. This is due to the fact that classical filters based on Fourier analysis assume the convergence of nonstationary functions which do not converge in practice [**20**].

The separation of frequency bands is used below when identifying bump events and when introducing them into the corresponding signal components of the vibration test profile being constructed. Then, the test profile components are summed to form an entire vibration test signal. It is desirable that an error introduced by this two-stage procedure of decomposing and summing back is minimal. However, when the same input process was passed through a number of different band-pass filters and, then, the obtained outputs with erroneous smooth peaks presented by the thick curves in Figs. 5,a,b,c,d were summed back, the result (thick curve in Fig. 4,a) was far from the same time history, which was subjected to filtering (thin curve in Fig. 4,a).

The above means that apart from actual error in preserving bump events when moving them from road data to the vibration test profile, there is an additional error in Butterworth filter decomposing which is absent however in orthogonal wavelet decomposing because the latter is a numerical procedure that is reverted precisely. In accordance with the orthogonal wavelet theory, if all time histories of all wavelet levels are summed, the result is exactly the initial entire time history shown by the thin curve in Figs. 4,b **. That is why, to facilitate analysis of bump behaviour, not band-pass filtering but the wavelet decomposition has been chosen as a tool for separation of road vibration time history into signal components related to different vehicle subsystems.

---

* - *Note that time scales on the horizontal axes are different in Fig. 5,a, Fig. 5,b, Fig. 5,c, and Fig. 5,d, i.e. although these four plots seem to have similar periodicity, they nevertheless correspond to different frequency bands indicated in the figure captions*

** - *In practice, those wavelet levels with very small vibration amplitude are not taken into consideration and, hence, the result of summation shown by the thick curve in Fig. 4,b is a bit different from the initial data presented by the thin curve*

4. VIBRATION TEST PROFILE SYNTHESIS METHOD

4.1. Wavelet grouping

To obtain for each vehicle subsystem frequency band its own time history one should first calculate PSDs of all wavelet levels and present them on the same scale simultaneously with an initial PSD of the entire signal. Each of the wavelet levels corresponds to certain frequency range and retains all time domain features related to the bump events in the entire road data. The wavelet levels should then be grouped in such a way that each group corresponds to one of the frequency-bands of the whole PSD as those shown in Fig. 2. Some groups will combine several wavelet levels while others will consist of only one wavelet level. The grouping procedure has been discussed in [**11**] in more detail and a typical example is presented in Figs. 6,b,d,f,h, how an entire PSD has been decomposed into four groups. These results were obtained for the aforementioned Renault road data which included 327,660 time points. This means existence of 20 wavelet levels that were counted in the direction from high to low frequencies.

The 1^{st} wavelet level with highest frequencies felt to the right of the last PSD section in Fig. 2 and, therefore, has not been taken into further consideration. The 2^{nd} and 3^{rd} wavelet levels were taken together to make up Wavelet Group 1, whose PSD (Fig. 6,b) coincides with the fourth frequency band (from 22 to 60 Hz) of the entire road data PSD presented in Fig. 2. The 4^{th} wavelet level alone covered the third (from 13 to 22 Hz) frequency band of the road data PSD and, thus, was designated as Wavelet Group 2 (Fig. 6,d). How the subsequent wavelet levels up to 9^{th} were grouped and Wavelet Groups 3 and 4 were formed is shown in Table 1. All further wavelet levels starting from the 10^{th} were omitted because their frequency regions were located lower than the lowest present frequency in the road data PSD.

The same wavelet grouping was performed for the synthetic data file (Fig. 1,b) generated by the inverse Fourier transform of the road PSD. The power spectral density of Wavelet Group 1 constructed for this synthetic signal is presented in Fig. 6,b by the dotted curve and can be compared with the corresponding solid curve of the PSD of Wavelet Group 1 for the road data. It is clear from this comparison and from similar results for other wavelet groups that the synthetic background signal has precisely acquired all frequency features of the road data not only for the PSD of the entire signal (as was shown in Fig. 2) but also separately for each of the four PSDs of the wavelet groups obtained after wavelet decomposition of the entire signal. However, the situation changes if one compares the road data and the synthetic background signal not in the frequency domain but in terms of time history.

4.2. Identification of bump events in road data

To obtain statistically representative material about rare bump events, the time duration of the experimentally acquired road vibration signals should be much longer than in the case of ordinary PSD analysis. As an illustrative example for this paper, twenty repetitions of the aforementioned 40 second recordings, made for the Renault vehicle on the same track of a country road with the damaged surface were considered and placed one by one into a joint data record. Figures 7,a,c,e,g present time histories of all four wavelet groups obtained for these road data.

When the corresponding wavelet groups of the synthetic Fourier signal were obtained (Figs. 7,b,d,f,h) and compared with the road data, it became clear that, for Wavelet Group 4 with lowest frequencies, the road data regularly exhibit bump peaks (especially in positive direction) of such a height and regularity of appearance which are not inherent in the Fourier signal of the same group. Results for the other groups are similar, however the difference between bump behaviour in the road and synthetic Fourier data is smaller.

Evaluation of the above time history graphs is somewhat subjective and requires operation with very long time history files. Therefore, another view into the problem under consideration is recommended making use of probability density function (PDF). Particularly, tail behaviour of the PDF should be considered as this describes probability of large instantaneous values, i.e. how often large peaks due to bump events appear in the time history. A logarithmic scale is often used for vertical axis of PDF graphs [**5,10**] to represent low probability values better. Right PDF tail for all four wavelet groups of the road data (thick solid curves) and of synthetic Fourier signal (dotted curves) are presented in Figs. 6,a,c,e,g along with PSD sketches (Figs. 6,b,d,f,h) showing frequency content of every wavelet group*. There is always some overlap of frequencies between the wavelet levels and, hence, between the wavelet groups as well. That is why, when shown separately as in Figs. 6,b,d,f,h, the wavelet group spectra look wider than the corresponding frequency bands specified in Table 1 according to Fig. 2 and, then, presented in the captions to Figs. 5 and 7.

Table 1. Results of wavelet level grouping for seat guide vertical vibration of a Renault automobile

Wavelet Group	Wavelet levels included	Frequency band	PSD plot	Time history plot
No 1	2^{nd} and 3^{rd}	from 22 to 60 Hz	Figure 6,b	Figure 7,a
No 2	4^{th}	from 13 to 22 Hz	Figure 6,d	Figure 7,c
No 3	5^{th}	from 5 to 13 Hz	Figure 6,f	Figure 7,e
No 4	6^{th}, 7^{th}, 8^{th}, and 9^{th}	from 0.5 to 5 Hz	Figure 6,h	Figure 7,g

It can be seen from Figs. 6,a,c,e,g that the PDF tails of the synthetic Fourier signal (dotted curves) always lie lower than those of the road data whose PDF tails (thick solid curves) are wider and longer. This means that a peak with height of 2 r.m.s (σ) values or more has several times less probability of occurrence in the synthetic Fourier signal than in the road data. This difference between the road data and the synthetic signal is largest for Wavelet Group 4, and this fact will be of prime importance in later considerations.

For example, in Fig. 6,g, acceleration value of 4.5 m/s^2 (that is about 3.5σ) has a probability of occurrence 100 times higher for the road data than for the Fourier signal. Since the data record length is restricted in numerical analysis, one cannot actually obtain probabilities less than L^{-1} where L is a number of data points in the time history under consideration. That is why we do not know what would be the probability of occurrence of 5.7 m/s^2 acceleration value (that is 4.6σ) in the synthetic Fourier signal and how many times it is less than the 0.0001 probability observed for the same acceleration value in the road data. Instead, one should compare not probabilities but peak acceleration values corresponding to the same 0.0001 probability of occurrence in the road and in the Fourier data. In this instance, these peak acceleration values were 4.5 m/s^2 and 5.7 m/s^2 making up a substantial difference.

4.3. Extraction of bump events from the road data and superimposition unto the time histories of the wavelet groups of the Fourier-generated signal

Comparison of the road and synthetic Fourier data discussed in the previous section reveals differences in behaviour related to bump events. This suggests that a specific action for the purpose of bump modeling should be undertaken for certain wavelet level group signals in addition to conventional PSD simulation. These somehow corrected wavelet groups can then be summed along with other wavelet groups (if any) which contained no essential bumps in the road data and for which no corrections to the Fourier synthetic signal were made. This summation will reconstruct the entire vibration test profile.

---

* *Note that the vertical axis scale in Fig. 6,h is different from that in Figs. 6,b,d,f.*

Each of the wavelet groups defined by the grouping procedure established in Section 4.1 is considered separately. It was shown in [**11**] by numerical examples that this makes a bump event much more distinguishable than in the time history of the entire road data because contributions from other wavelet levels (i.e. signals corresponding to other vehicle subsystem frequency bands) are not superimposed on the bump event under consideration and, thus, do not cover it. Here it is supposed that a bump event is occurring in only one of the wavelet groups whereas nothing causing bumps happened in other wavelet groups at the same moment of time. A more complicated case is considered in the next section of the paper, when a bump event is related for two or more wavelet groups simultaneously and, therefore, some synchronization of what is taken from different groups is necessary.

In the case of no synchronization between the wavelet groups, a point is considered a bump event if the wavelet group time history has a maximum or minimum exceeding a certain boundary value which is prescribed such that it can only be reached by essentially high peaks. Experience suggests that this boundary value may be taken equal to 1.5-2.5 times the r.m.s value σ.

Assuming that any bump event takes some time to be developed from background vibration and, then, must be accompanied by a monotonic decay process depending on the level of system damping, the main peak found in road data and taken to the vibration test profile should be accompanied by a few preceding and subsequent waves. A number of these waves is defined by going forward and backward of the main peak and comparing heights of maxima and minima with the preceding ones. The process is stopped when the next maximum is higher (or minimum is lower) than the former one. This is considered as an indication of the fact that the decay process is finished and a new increase in the oscillation amplitude started to develop.

When a bump event is identified in the wavelet group of the road data, it should be placed in the same wavelet group of the synthetic Fourier signal in such a way as to cause the least possible disturbance to the latter. For this purpose, the time history section of the bump is moved along the whole time history of the synthetic signal and compared with it in terms of root-mean-square difference in each of the possible positions. Then, at the point where this difference is smallest, the bump section substitutes the similar and equal in length section found in the background synthetic signal.

If a high compression value (ratio between the initial length of road data prescribed and the required length of the vibration test profile) is specified, then there might be no room to accommodate into the background Fourier time history all the bump events extracted from the road data (especially for wavelet groups with lower frequencies). To cope with such a situation and to ensure that the most influential bumps are included, the bump events found in a particular wavelet group are ranked in descending order before being put one by one into the corresponding wavelet group of the test profile signal.

When all wavelet groups (i.e. frequency bands) requiring correction have been considered and all bump events for each of the groups have been identified and put unto the Fourier synthetic wavelet group signals, this is followed by summation of the wavelet groups. As a result, a background test signal constructed by inverse Fourier transform of the road PSD upgrades into the vibration test profile representative of bump behaviour as well as of the prescribed PSD shape. The entire method described above was called Mildly Nonstationary Mission Synthesis (MNMS) in Ref [**21**] and a flow-chart of the procedure can be found in this former paper of the authors.

4.4. Analysis of vibration test profile PDFs and synchronisation of bump events.

When investigating bump event differences between corresponding wavelet groups of the road data and Fourier-generated background signals, probability density functions and, particularly, their tail behaviour were used in Section 4.2. This approach was proved effective and, here, it is employed for vibration test profile signals to evaluate performance of the developed algorithm.

First, PDFs of vibration test profiles were computed at the intermediate stage of considering the wavelet groups separately. The results obtained are presented by the thin solid curves in Figs. 6,a,c,e,g. These vibration test profile PDF tails are so close to the PDF tails for the road data (thick curves on the same plots) that the thin curve is covered by the thick one almost everywhere. This means that introduction of bump events into the Fourier-generated synthetic signals of the wavelet groups has changed their PDF tails dramatically moving them from the initial unsatisfactory dotted curves in Figs 6,a,c,e,g towards perfect coincidence with the thick curves of the PDF tails for the road data prescribed.

However, the comparison of the PDF tails of the test signal and the road data was less satisfactory after summation of the wavelet group signal components into an entire vibration test profile. As seen from Fig. 8,a for the vibration test profile as a whole, the probability density function produced by the new synthesis algorithm took an intermediate position between those of the road data and that produced by the traditional technique based on PSD considerations only. Since the results for each of the wavelet groups were perfect, this subsequent decrease in precision for a summation signal can only be attributed to the fact that something was missing in correlation of different wavelet groups.

As explained in Section 4.3, in the base procedure bump events were extracted from a certain wavelet group signal independently of what occurred at the same moment of time on other wavelet groups. Then, a bump event from the particular wavelet group was placed to the most appropriate position at the background Fourier-generated signal of the same wavelet group and, again, no consideration has been given to what was happening with the other wavelet groups. In so doing, if any relation existed in the road data between two bumps on different wavelet group signals, this relation would be broken.

The time positions where the first and second bumps are placed on the first and second wavelet groups were dictated by corresponding wavelet groups in the Fourier signal which are absolutely independent. Hence, there is no relationship between the two bumps under consideration after they were moved from the road data to the vibration test profile constructed. This had to be dealt with by some action of synchronisation. Bump events that occurred in the road data on different wavelet groups at the same (or very close) moments of time should be kept together when introduced into vibration test profile wavelet groups.

One possible synchronisation algorithms was established as follows. Experience of wavelet grouping and bump events identification in various road data has suggested that in most cases a main wavelet group can be nominated, which is indicative of an intensive bump behaviour exceeding that of all other groups. In the Renault country road data under consideration this was Wavelet Group 4. One can see this from Fig. 7 where the difference between the road data and the Fourier-generated synthetic time histories is higher for Group 4 than for the other groups.

This main wavelet group was subjected to bump event extraction procedure, ahead of other groups. The bumps were not only extracted from the road data but their position, i.e. time moments of the bump transient wave beginning and the end, was memorised by the algorithm for future reference. Then, when considering other groups (not main) each of the bump events extracted from

them was compared in terms of its position with the positions of all bump events in the main group one by one.

If a bump event in a non-main group has fallen within, or has covered, the time interval of some bump event in the main group (or, at least, the end/beginning of one of these two bumps occurred between the beginning and the end of the second bump event), then the bump extracted from the non-main group should be placed on the background Fourier-generated signal differently than it was explained above for the algorithm with no synchronisation. Its position should not be chosen based on root-mean-square difference, but the observed relation between the two bump events in the main and non-main group must be respected by directing the non-main group bump to such a position in the non-main group time history where it would have exactly the same (as was in the road data) shift in time compared to the position of the relevant bump in the main group time history.

5. RESULTS OF CONSTRUCTING VIBRATION TEST PROFILES BY DIFFERENT SYNTHESIS PROCEDURES AND FOR VARIOUS COMPRESSION RATIOS

The synchronisation procedure for locating bump events in subsequent wavelet groups verifying their position against corresponding bump events in the main group has been implemented for the same Renault automobile data which was used in the example of non-synchronised algorithm presented in Fig. 8,a. The synchronisation algorithm has produced a vibration test profile with the PDF tail (see Fig. 8,b) much closer to that of the road data.

The further improvement, provided by the synchronisation algorithm compared to the non-synchronisation case, was similar to the improvement already provided by the non-synchronised algorithm compared to PSD simulation with no consideration of bump events. Table 2 presents the acceleration values of time history peaks corresponding to various probabilities of occurrence for all four PDFs under consideration: obtained by PSD simulation, by the new algorithm with no synchronisation, by the new algorithm enhanced with synchronisation, and for the road data PDF prescribed.

Table 2. Peak heights corresponding to different probabilities of peak occurrence

Probability of peak occurrence	PSD simulation		No synchronisation		Synchronisation		Road data	
	m/s^2	%	m/s^2	%	m/s^2	%	m/s^2	%
0.001	5.5	81	6.5	96	6.8	100	6.8	100
0.0001	6.6	73	7.9	87	8.7	96	9.1	100
0.00001	7.5	71	8.7	83	10.0	95	10.5	100

It is seen from these results that for 0.001 probability of peak occurrence the synchronisation algorithm provided perfect simulation matching the peak height observed in the road data. The non-synchronisation algorithm was good as well losing just 4% of the peak height, whereas peaks in the time history of PSD simulation were restricted to 81% of those occurring in the road data. For 10 times lower probability (0.0001), results by the synchronisation algorithm are 96% of the road peak value whereas the PSD simulation dropped to 73% and non-synchronisation appeared to be 87%, i.e. slightly more than the half-way between the PSD simulation and the enhanced version of new algorithm. For the lowest probability value (0.00001) results by the synchronisation procedure are still acceptable (95% of road data) whereas the PSD simulation and the non-synchronisation algorithm degraded furthermore to 71% and 83% correspondingly.

Thus, there is an obvious need to maintain the relation between bump events occurring on different wavelet groups at close moments of time by introducing them jointly into the vibration test profile. This synchronisation procedure was used for the further plots in Fig. 8 and in all following computations. Figure 9,a presents time history of one run of the Renault automobile on the same country road test track which was considered earlier, when several runs were joined into one data file. There are three apparent bump events at 6.2 sec, 8.4 sec, and 34.2 sec moments of time marked as B1, B2 and B3 at the top of the plot frame in Fig. 9,a. Of course, many other bumps, which cannot be observed in this entire signal record, have been detected by the algorithm at particular wavelet groups.

The aforementioned three bump events are distinguishable in the vibration test profile constructed, now at 8.5 sec, 29 sec, and 18.1 sec moments of time (see Fig. 9,b). Each of the events has undergone certain transformation because some of the wavelet groups (where a bump has been detected) contribute with their time history section taken from the road data, whereas others (where there were no bumps at this time) contribute with a section of synthetic Fourier-generated signal. Hence, bump events in the vibration test profile do not look exactly the same as in the road data, however their heights and essential features, like number of waves in the bump event, were simulated.

For example, the bump event B1 in the road data at 6.2 sec had a height of 9.6 m/sec^2 and consisted of just one extreme wave. The former was retained in the vibration test profile at 8.5 sec position with height of 7.8 m/sec^2. Another bump event (B3) at 34.2 sec of the road data was completely different with three subsequent extreme waves with heights 6.2 m/sec^2, 8.2 m/sec^2, and 8.95 m/sec^2. One can see that these three wave event has been simulated in the vibration test profile at 18.1 sec moment with heights 6.3 m/sec^2, 8.2 m/sec^2, and 8.8 m/sec^2.

As was mentioned in Introduction section, the main objective of this research was to find ways of producing vibration test profiles several times shorter then the road data record prescribed. Figures 9,c,e show vibration test profiles with increasing compression value, i.e., two and three times shorter than the road record. These were compared with Fourier synthetic signals of the same length (Figs. 9,d,f). In so doing, one can see the distinguishable peaks that have been moved from the road to the vibration test profile but were missed in the Fourier signals presented at the right.

As discussed in Section 4.3, the shorter vibration test profile is required, the more difficult is to properly simulate bump behaviour because not all bump events found in the road data can be accommodated into the vibration test profile with the space available for bump placement decreasing. For instance, one of the aforementioned three bump events, particularly B2 (occurred at 8.4 sec in the road data), was absent in the vibration test profile with the compression value of 3 (see Fig.9,e). Thus, some degradation of the vibration test profile quality is an inevitable payment for the requirement to have a test profile several times shorter then the road measurements. However, consideration of probability density functions of these shorter test profiles in comparison with PDFs of the road data and the Fourier simulation (see Fig. 8,c,d) justifies that the method developed still provides satisfactory closeness to the road data and is much better than the traditional PSD simulation would be.

6. CONCLUSIONS

The research described in this paper can be summarized as follows:

1. The orthogonal transform performed by means of Daubechies wavelets was used as a filtering tool for analysing bump (shock transient) events in automobile vibration time histories. This approach facilitates the task of bump event identification because vibration signals of individual frequency bands related to different vehicle subsystem behaviour were separated.

2. A wavelet grouping procedure has been introduced where summation is carried out of time history signals of all those wavelet levels whose PSDs are covered by the particular frequency band.
3. An unsynchronised and a synchronised algorithms for generating vibration test profiles have been developed. An example have been presented of the application of the method to car passenger seat guide acceleration data, and compression ratios of up to 3 have been achieved. The synchronisation algorithm has been tried for various data and research is continuing towards establishing few other synchronisation algorithms.
4. The techniques described in this paper permit the definition of vibration test profiles which maintain probability of occurrence of high-amplitude bump events to within few percent difference from the probability of their occurrence in the original road data.

The paper results should find numerous automotive applications including laboratory testing and numerical simulations. Further research is under way to develop algorithms for long-time black box recorders for summarising the vehicle vibration environment.

7. ACKNOWLEDGEMENTS

The research described in this paper was financed by the European Commission as part of the activities of Brite-Euram Project BE-97-4186 SCOOP "Seat Comfort Optimisation Procedure". The authors would like to thank Mohamed Karouia and Laurent Richard of Renault S.A. for providing the road data for this study and for aiding in data interpretation.

REFERENCES

1. Baddeley, A. *Human Memory: Theory and Practice*, 1997 (Psychology Press, Hove, East Sussex).
2. Shinozuka, M. and Jan, C.-M., Digital simulation of random processes and its applications. *Journal of Sound and Vibration*, 1972, **25**, 111-128.
3. Crolla, D.A., Soliman, A., Elsayed, F.M., et al., Experimental results from a slow-active suspension system. *International Journal of Vehicle Design*, 1993, **14** (2-3), 226-245.
4. Sherratt, F., Current applications of frequency domain fatigue life estimation. *Environmental Engineering*, 1996, December, 12-20.
5. Steinwolf, A., Shaker simulation of random vibration with a high kurtosis value. *Journal of the IES*, 1997, May/June, 33-43.
6. Steinwolf, A., Approximation and simulation of probability distributions with a variable kurtosis value, *Computational Statistics and Data Analysis*, 1996, **21** (2), 163-180.
7. Smallwood D. O., Generation of stationary non-Gaussian time histories with a specified cross-spectral density. *Shock and Vibration*, 1997, **4**, 361-377.
8. Merritt, R.G., A stochastic model for the pulse method – Part 2: Random part, In *Proceedings of the 43rd IES Annual Technical Meeting*, Los Angeles, 1997, 121-129.
9. Connon, W.H., Comments on kurtosis of military vehicle vibration data. *Journal of the IES*, 1991, September/October, 38-41.
10. Charles, D., Derivation of environment descriptions and test severities from measured road transportation data, *Environmental Engineering*, 1992, December, 30-32; 1993, March, 25-26.
11. Giacomin, J.A., Steinwolf, A., Staszewski, W.J. A vibration mission synthesis algorithm for mildly nonstationary road data. In *Proceedings of the 6th ATA International Conference*, Florence, 1999.
12. Giacomin, J. and Bracco, R., An experimental approach for the vibration optimisation of automotive seats. In *Proceedings of the* 3rd *ATA International Conference on Vehicle Comfort and Ergonomics*, Bologna, 1995.
13. Chui, Ch. K., *An Introduction to Wavelets, Analysis and its Applications*, 1992, Vol. 1 (Academic Press, Boston).

14. Newland, D.E., *Random Vibration, Spectral and Wavelet Analysis*, 1993 (Longman, New York).
15. Staszewski, W. J. and Giacomin, J.A., Application of the wavelet based FRFs to the analysis of nonstationary vehicle data. In *Proceedings of the 15th International Modal Analysis Conference*, Orlando, 1997.
16. Lee, S.K. and White, P.R., Application of wavelet analysis to the impact harshness of a vehicle, *Proc. Instn Mech. Engrs, Part C, Journal of Mechanical Engineering Science*, 2000, **214** (C11), 1331-1338.
17. Donoho, D. and Johnstone, I., Ideal denoising in an orthonormal basis chosen from a library of bases. *C R Acad. Sci. Paris*, Série I 1994, **319**, 1317-1322.
18. Staszewski, W. J., Wavelet based compression and feature selection for vibration analysis. *Journal of Sound and Vibration*, 1998, **211** (5), 735-760.
19. Hamming, R.W., *Digital Filters*, 1983, (Prentice-Hall, Englewood Cliffs, NJ).
20. Mallat, S, A *Wavelet Tour of Signal Processing*, 1998, (Academic Press, San Diego).
21. Giacomin, J.A., Steinwolf, A. and Staszewski, W.J., An algorithm for mildly nonstationary mission synthesis (MNMS). *Engineering Integrity*, 2000, **7**, 44-56.

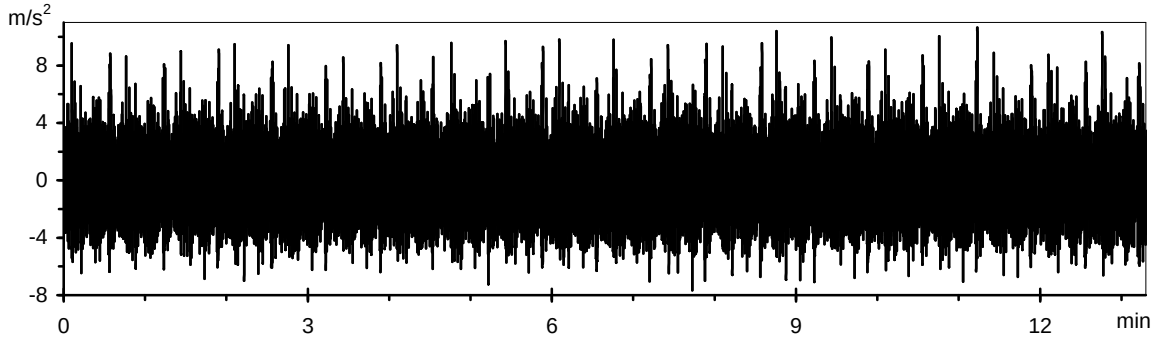

a) Acceleration time history measured in a Renault automobile on a country road test track

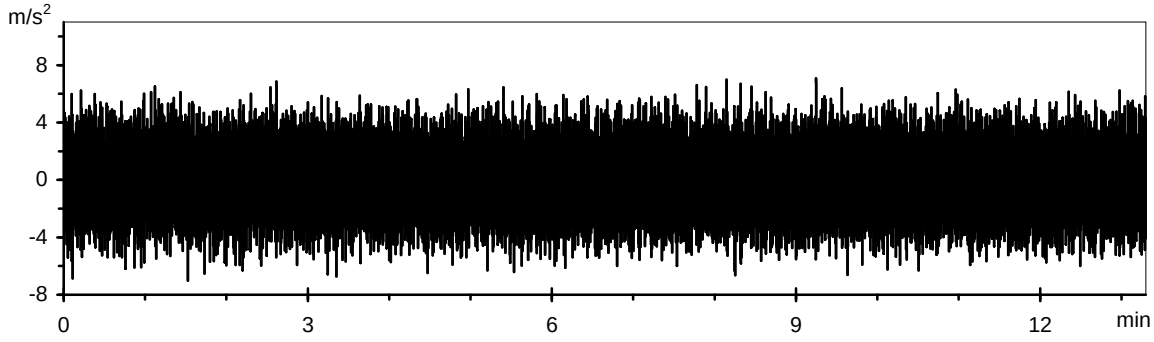

b) Fourier-synthesised time history with the same PSD as the road data above

Fig. 1 Simulation of car body vertical vibration based only on power spectral density characteristic

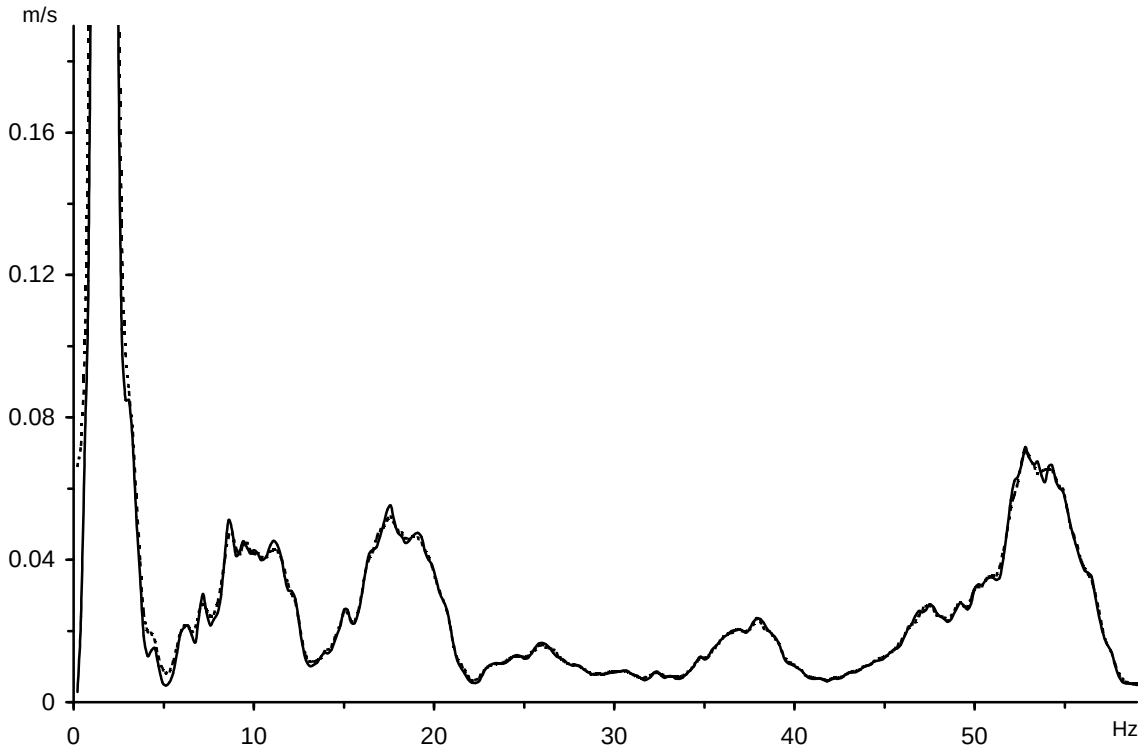

Fig. 2 Power spectral densities of the experimental road data (solid curve) and the synthetic Fourier signal (dotted curve).

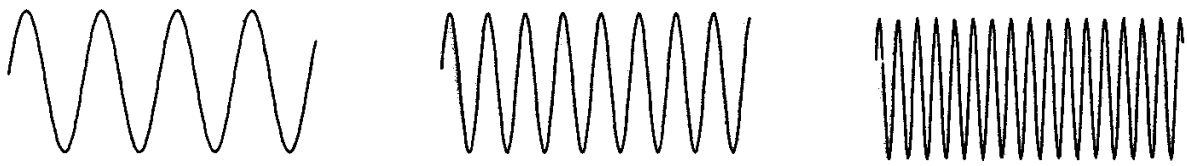

a) Fourier analysis – trigonometric functions

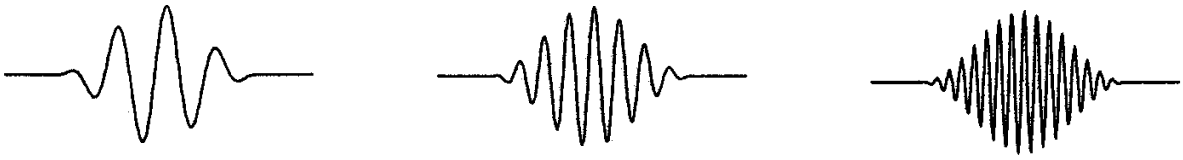

b) Windowed Fourier transform – decaying trigonometric functions

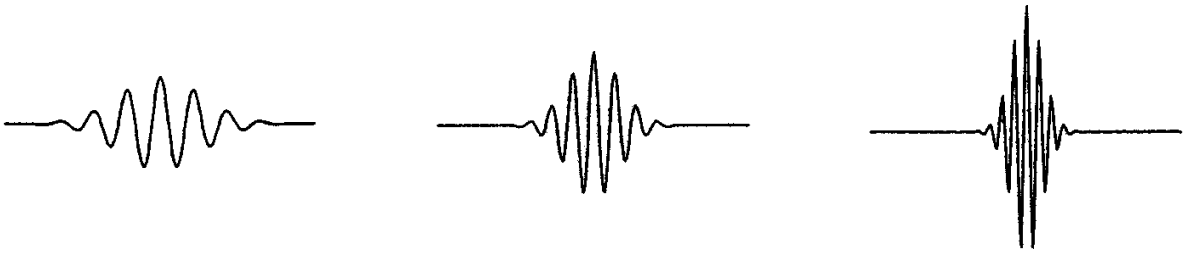

c) Wavelet analysis – wavelets

Fig. 3 Elementary basic functions for signal decompositions.

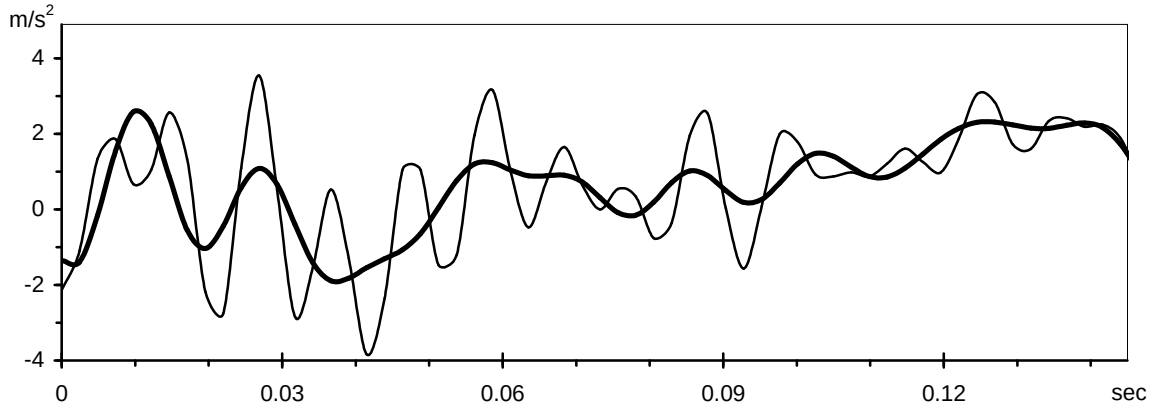

a) Decomposition by digital band-pass filter of the Butterworth type

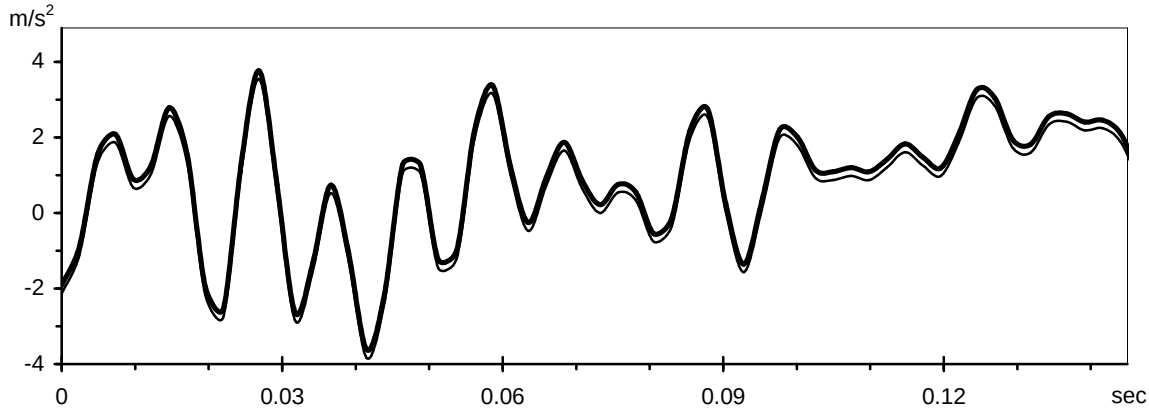

b) Decomposition by means of wavelet analysis

Fig. 4. Initial road data (thin curve) and results of reconstruction (thick curves) by summation of vibration components of different subsystem frequency bands separated by two decomposition methods.

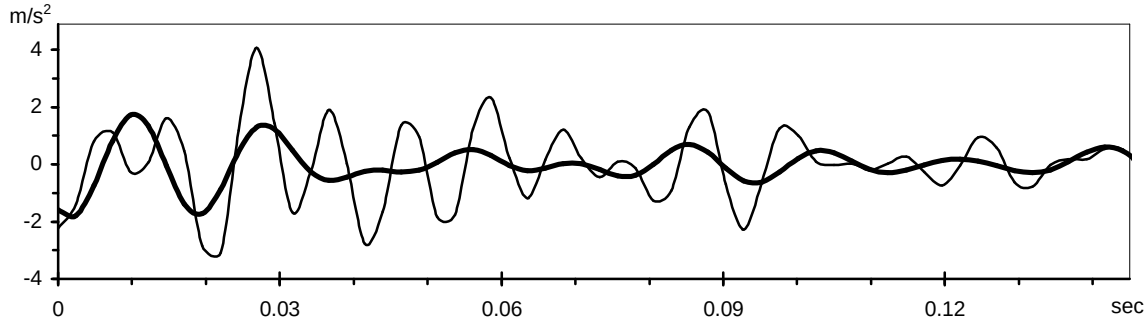

a) Time histories extracted for the frequency range between 22 and 60 Hz

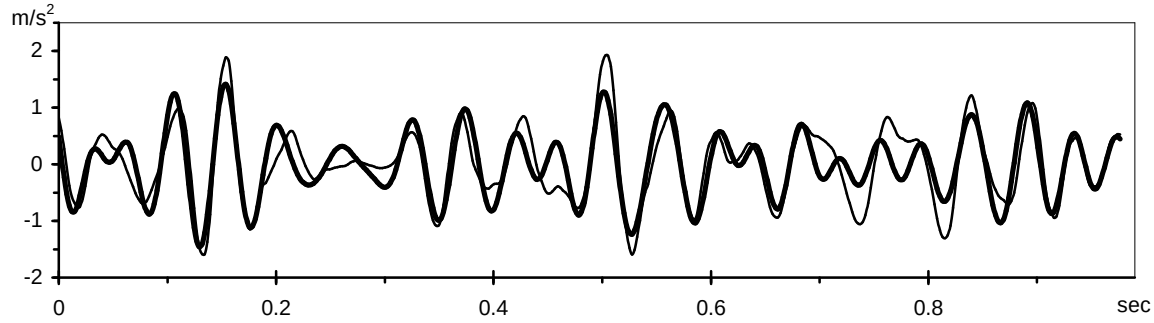

b) Time histories extracted for the frequency range between 13 and 22 Hz

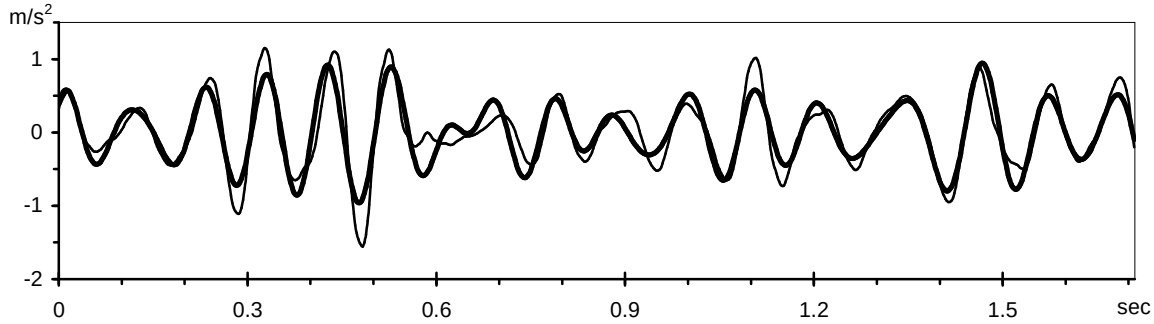

c) Time histories extracted for the frequency range between 5 and 13 Hz

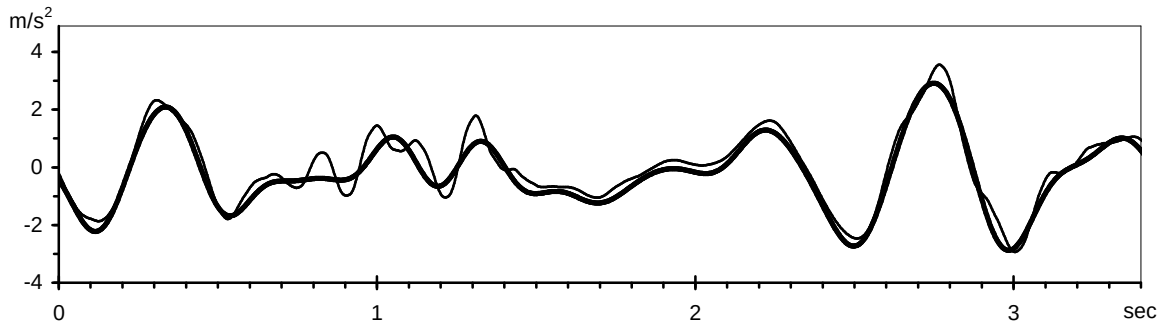

d) Time histories extracted for the frequency range between 0.5 and 5 Hz

Fig. 5 Smoothing peaks of shock events by digital filtering (thick time history curves) compared to those preserved by wavelet decomposition (thin curves)

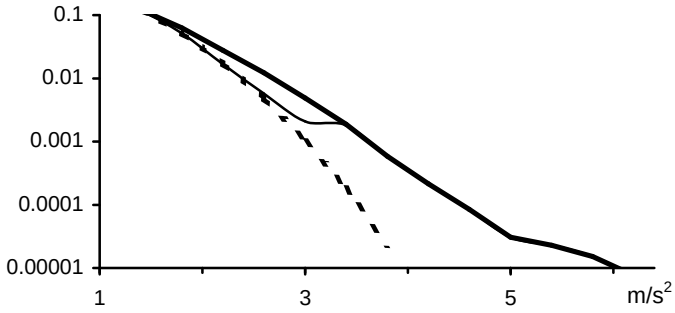

a) PDF right tail for Wavelet Group 1

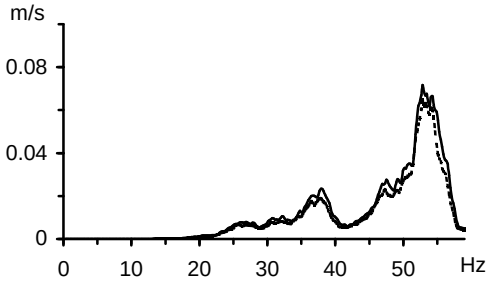

b) PSD for Wavelet Group 1

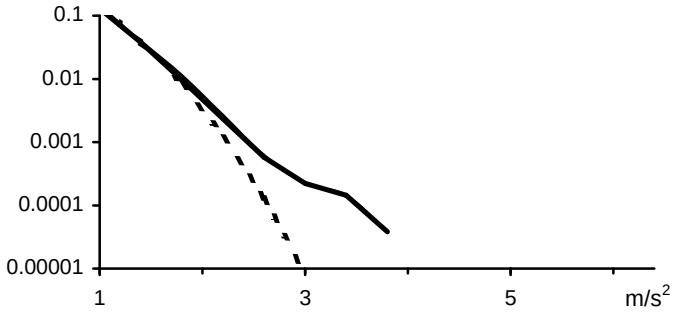

c) PDF right tail for Wavelet Group 2

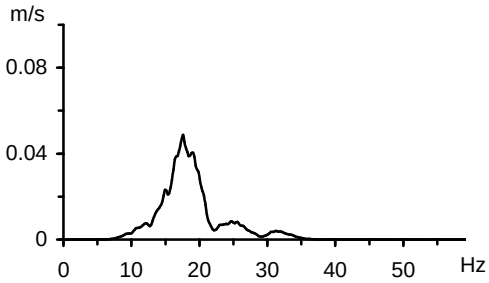

d) PSD for Wavelet Group 2

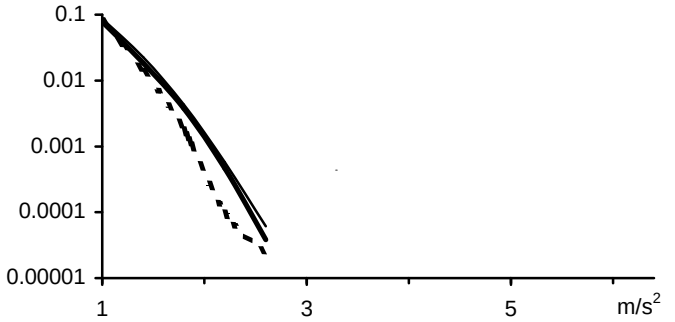

e) PDF right tail for Wavelet Group 3

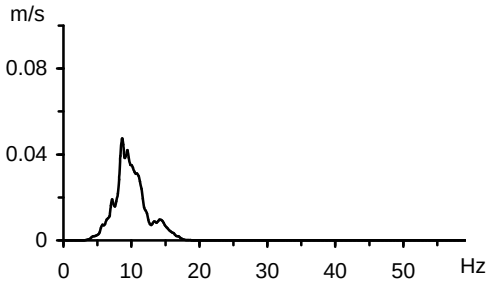

f) PSD for Wavelet Group 3

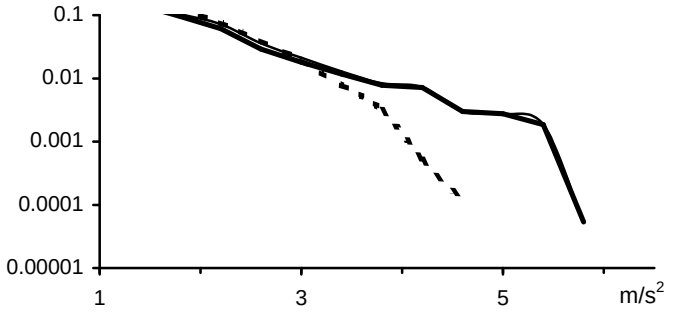

g) PDF right tail for Wavelet Group 4

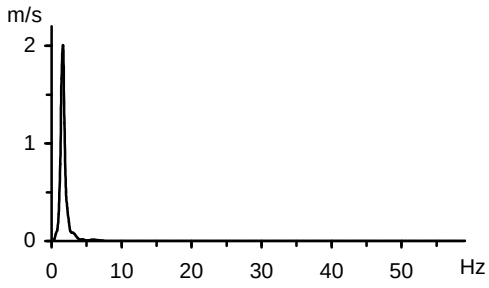

h) PSD for Wavelet Group 4

Fig. 6 Tails of probability density functions of road data (thick solid curves) and of synthetic Fourier signal (dotted curves) after decomposing into four wavelet groups with power spectral densities shown to the right.

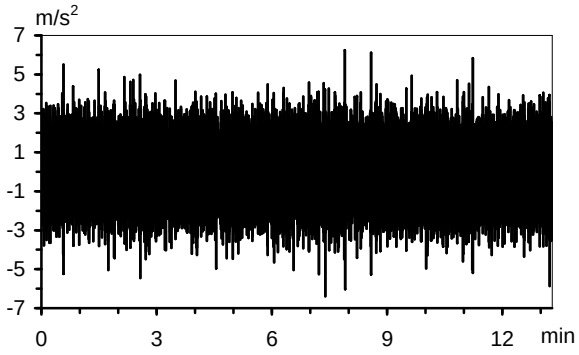

a) Group 1 road data (from 22 to 60 Hz)

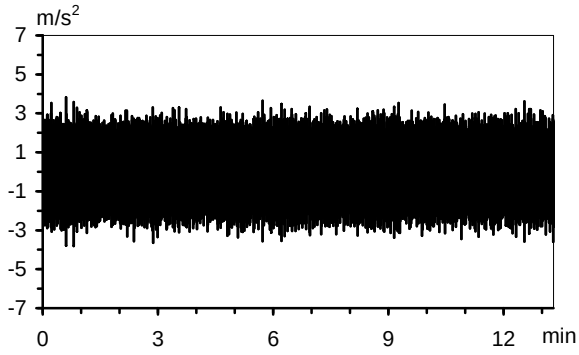

b) Group 1 Fourier signal (from 22 to 60 Hz)

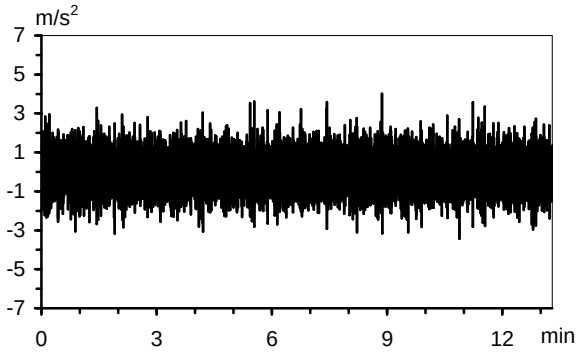

c) Group 2 road data (from 13 to 22 Hz)

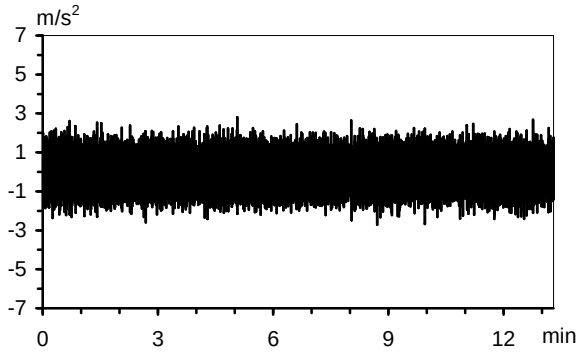

d) Group 2 Fourier signal (from 13 to 22 Hz)

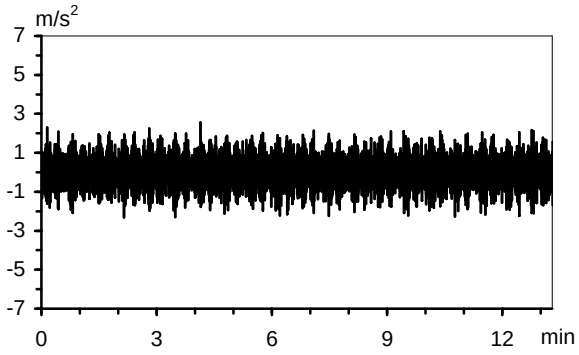

e) Group 3 road data (from 5 to 13 Hz)

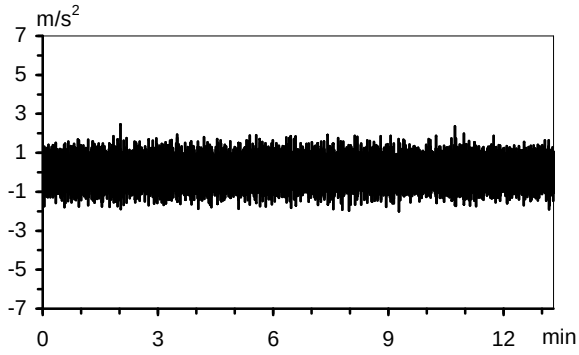

f) Group 3 Fourier signal (from 5 to 13 Hz

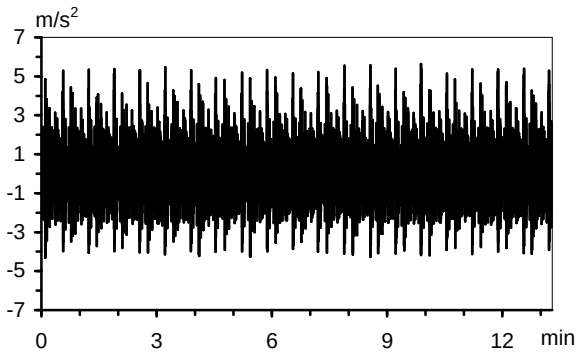

g) Group 4 road data (from 0.5 to 5 Hz)

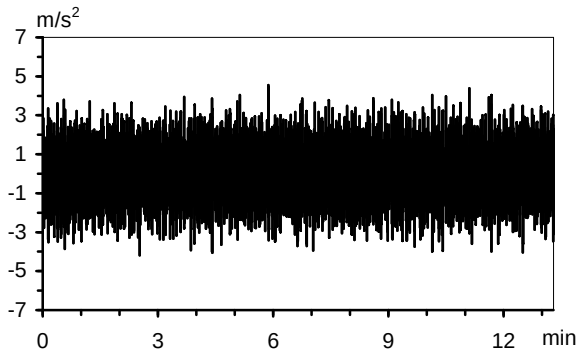

h) Group 4 Fourier signal (from 0.5 to 5 Hz)

Fig. 7 Time histories of road data (left) and synthetic Fourier signal (right) after decomposing into four wavelet groups.

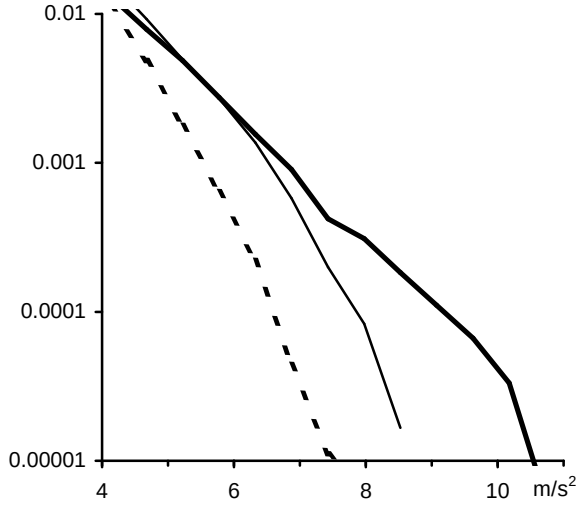

a) No synhronisation of shocks at wavelet groups

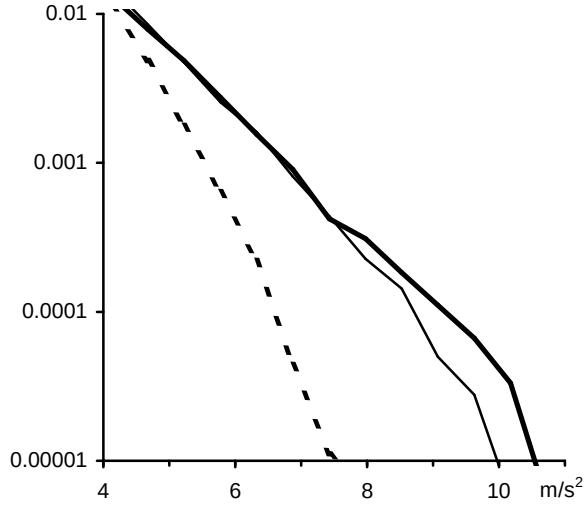

b) Shocks at wavelet groups were synchronised

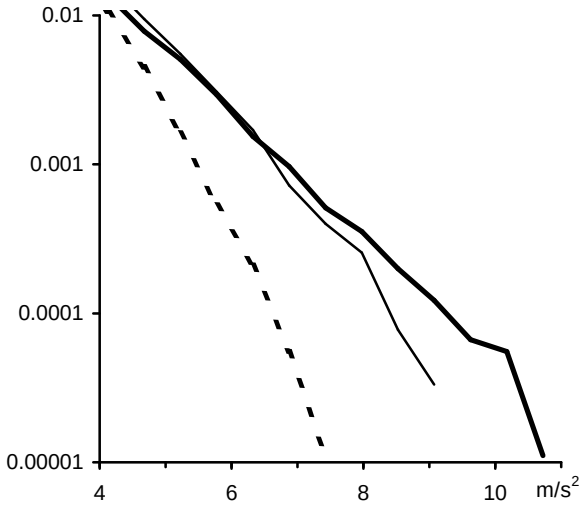

c) Two times compression with synhronisation

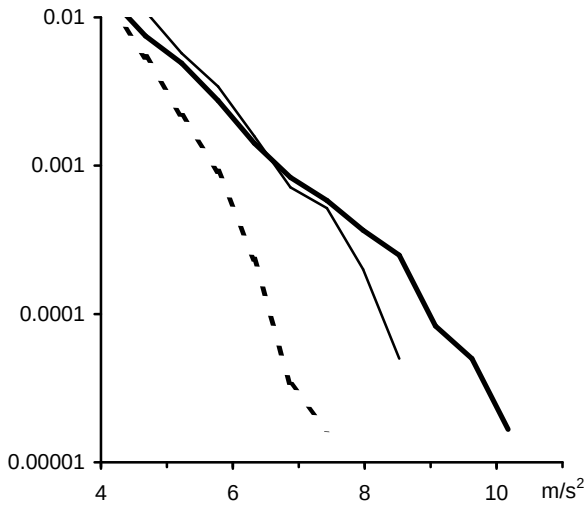

d) Three times compression with synhronisation

Fig. 8 Tails of probability density functions of road data (thick solid curves), synthetic Fourier signal (dotted curves) and vibration test profile constructed (thin solid curves).

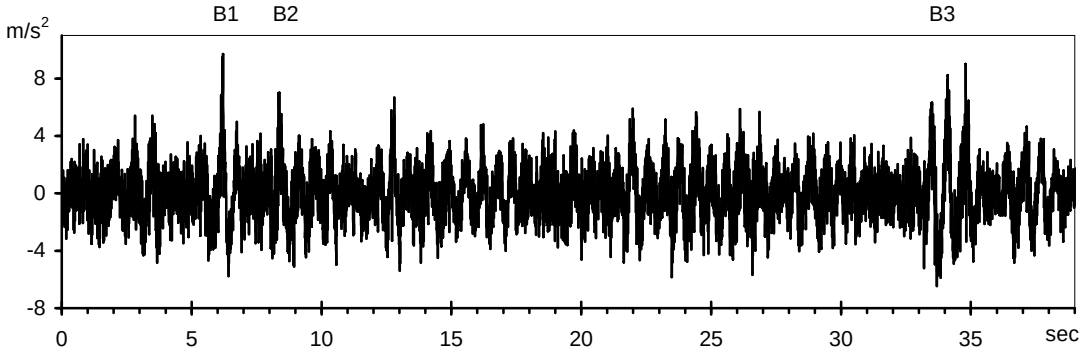

a) Time history of the road data

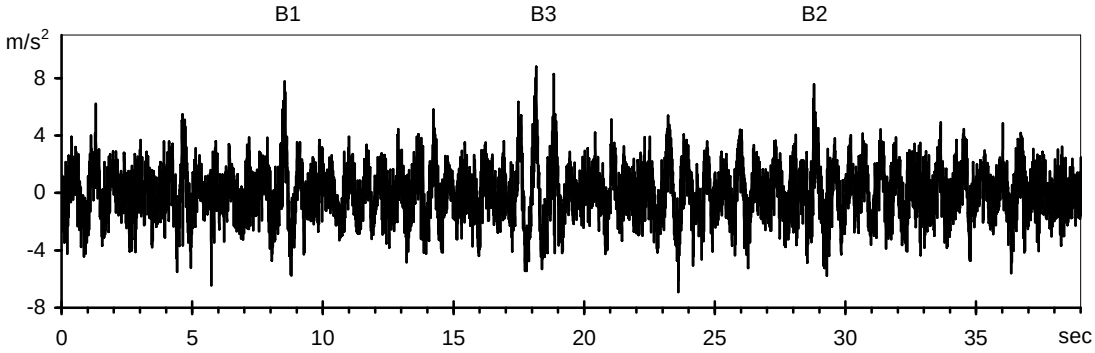

b) Vibration test profile with no compression

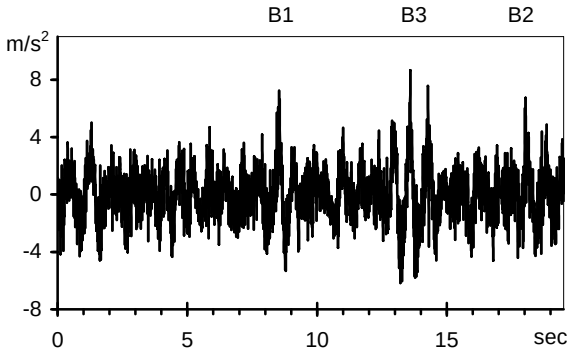

c) Test profile with 2 times compression

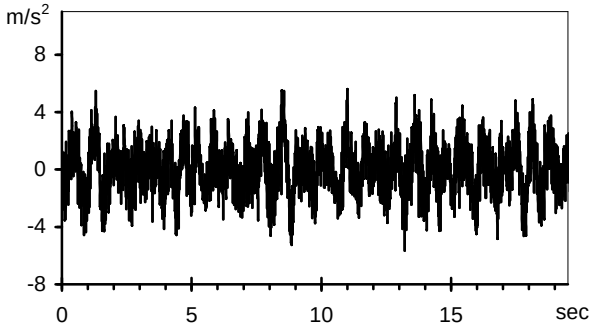

d) Fourier signal with 2 times compression

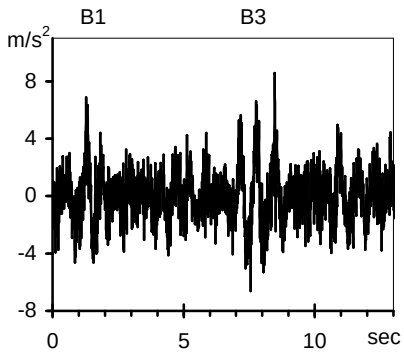

e) Test profile with 3 times compression

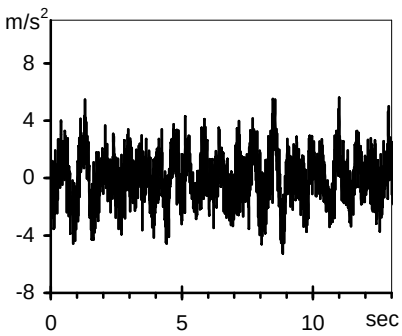

f) Fourier signal with 3 times compression

Fig. 9 Results of simulation for a Renault automobile on a country road test track.